J. Biochem. **137**, 569–578 (2005)
DOI: 10.1093/jb/mvi075

Stabilization Due to Dimer Formation of Phosphoribosyl Anthranilate Isomerase from *Thermus thermophilus* HB8: X-Ray Analysis and DSC Experiments

Junichiro Taka[1], Kyoko Ogasahara[2], Jeyaraman Jeyakanthan[1], Naoki Kunishima[1], Chizu Kuroishi[1], Mitsuaki Sugahara[1], Shigeyuki Yokoyama[1,3,4] and Katsuhide Yutani[1,*]

[1]RIKEN Harima Institute at SPring8, 1-1-1 Kohto, Mikazukicho, Sayo, Hyogo 679-5148; [2]Institute for Protein Research, Osaka University, 3-2 Yamadaoka, Suita, Osaka 565-0871; [3]RIKEN Genomic Sciences Center, 1-7-22 Suehiro, Tsurumi, Yokohama 230-0045; and [4]Graduate School of Science, the University of Tokyo, 7-3-1 Hongo, Bunkyoku, Tokyo 113-0033

Received December 30, 2004; accepted February 11, 2005

The crystal structure of phosphoribosyl anthranilate isomerase (PRAI) from *Thermus thermophilus* HB8 (*Tt*PRAI) was solved at 2.0 Å resolution. The overall structure of *Tt*PRAI with a dimeric structure was quite similar to that of PRAI from *Thermotoga maritima* (*Tm*PRAI). In order to elucidate the stabilization mechanism of *Tt*PRAI, its physicochemical properties were examined using DSC, CD, and analytical centrifugation at various pHs in relation to the association-dissociation of the subunits. Based on the experimental results for *Tt*PRAI and the structural information on *Tt*PRAI and *Tm*PRAI, we found that: (i) the denaturation of *Tt*PRAI at acidic pH is correlated with the dissociation of its dimeric form; (ii) the hydrophobic interaction of *Tt*PRAI in the monomer structure is slightly greater than that of *Tm*PRAI, but dimer interface of the *Tm*PRAI is remarkably greater; (iii) the contributions of hydrogen bonds and ion bonds to the stability are similar to each other; and (iv) destabilization due to the presence of cavities in *Tt*PRAI is greater than that of *Tm*PRAI in both the monomer and dimer structures.

Key words: differential scanning calorimetry, phosphoribosyl anthranilate isomerase, protein interaction, protein stability, X-ray analysis.

Abbreviations: PRAI, Phosphoribosyl anthranilate isomerase; *Tt*PRAI, PRAI from *Thermus thermophilus* HB8; *Tm*PRAI, PRAI from *Thermotoga maritima*; *Ec*PRAI, PRAI (C-terminal) domain of bifunctional enzyme from *Escherichia coli*; DSC, differential scanning calorimetry; ASA, accessible surface area; rmsd, root mean square deviation.

Proteins from thermophiles are remarkably stable compared with homologous proteins from mesophiles. To date, three-dimensional structures of many proteins from various thermophiles have been determined and compared in order to elucidate the mechanism of the extremely high stability of these proteins. Although many stabilization factors responsible for high stability have been proposed based on structural features (*1–3*), the molecular origin for the high stability of thermophile proteins remains to be answered. To address these questions, it is important to characterize the physicochemical properties of thermophile proteins in solution, and the stability should be analyzed on the basis of the structural features in comparison with their counterparts from mesophilic organisms. The results might provide valuable insight into the creation of stably folded proteins by protein engineering.

Phosphoribosyl anthranilate isomerase [EC 5.3.1.24] (PRAI) catalyzes the conversion of *N*-(5′-phosphoribosyl)-anthranilate to 1-(*o*-carboxyphenylamino)-1-deoxyribulose 5-phosphate in the tryptophan biosynthesis pathway. Two crystal structures of PRAI have been reported: one from a mesophile *Escherichia coli* (*4*) and another from a hyperthermophile *Thermotoga maritima* (*5*) that has a maximum growth temperature of 90°C (*6*). PRAI from *E. coli* (*Ec*PRAI) occurs as the C-terminal domain of a bifunctional enzyme, which is a monomer, whereas that from *T. maritima* (*Tm*PRAI) is a homodimer. Although the structure of *Tm*PRAI has a complete TIM barrel fold (*5*), the helix α5 in *Ec*PRAI is replaced by a loop. The subunits of *Tm*PRAI associate *via* the N-terminal faces of their central β-barrels through multiple hydrophobic interactions. The side chains of the N-terminal Met and the C-terminal Leu of both subunits are immobilized in a hydrophobic cluster at the subunit boundary. Especially, the sequential hydrophobic residues (Leu50-Pro51-Pro52-Phe53-Val54) in *Tm*PRAI dimer protrude reciprocally into the interior of the β-barrel of the neighboring subunit. Its hydrophobic amino acid sequence has been reported to be mainly responsible for the higher thermostability of *Tm*PRAI (*5*), because equivalent hydrophobic residues had not been observed in PRAIs from mesophiles at that time (*7*). The oligomerization of several subunits is one of the important factors responsible for the extremely high stability of proteins from hyperthermophiles (*1*, *8–13*).

*To whom correspondence should be addressed. Tel: +81-791-58-2937, Fax: +81-791-58-2917, E-mail: yutani@spring8.or.jp

Due to the recent abundance of Genome Projects, a large number of PRAI sequences have become available from many different sources. The alignment of all PRAI sequences from the Swiss Prot data bank (June 2004 release) shows that PRAIs from mesophiles, such as *Geobacter metallireducens*, *Nitrosomonas europaea* ATPC, *Pseudomonas fluorescens* PfO-1, *Neisseria meningitidis* Z2491 and, *Pseudomonas putida* KT2440, for which the optimal growth temperatures are lower than 37°C, have the same sequences from Leu50 to Val53 (LPPFV) as those of *Tm*PRAI. This fact indicates the possibility that these mesophile proteins are present as homodimers and that the hydrophobic sequence of LPPFV is not specific characteristic of thermophile proteins such as *Tm*PRAI.

Recently, we determined the crystal structure at 2.0 Å resolution of PRAI from *Thermus thermophilus* HB8 (*Tt*PRAI), which is an extremely thermophilic bacterium with a maximum growth temperature of 85°C. The overall structure of *Tt*PRAI is quite similar to that of *Tm*PRAI with a dimeric structure. *Tt*PRAI also has a hydrophobic protrusion at the subunit interface, which is similar to that of *Tm*PRAI. Therefore, in order to elucidate the role of the protrusion, the stability of *Tt*PRAI has also been investigated by differential scanning calorimetry (DSC) in the acidic range in relation to the association–dissociation of the subunits. In this paper, the thermostabilization mechanism of PRAIs from thermophiles will be discussed on the basis of the crystal structures of proteins from mesophilic, extreme thermophilic, and hyperthermophilic organisms.

MATERIALS AND METHODS

Purification of TtPRAI—*Tt*PRAI was over expressed in *E. coli* strain BL21 (DE3) containing only the *trp*F gene from *T. thermophilus* HB8. The *E. coli* strain was routinely grown at 37°C in 2.3 liters of LB medium containing 50 mg liter^{-1} ampicillin for 20 h. The cells were harvested by centrifugation at 6,500 rpm for 5 min, suspended in 20 mM Tris-HCl, pH 8.0, containing 500 mM NaCl and 5 mM 2-mercaptoethanol, and disrupted by sonication. The supernatant was heated at 70°C for 10 min. After heat treatment, the cell debris and denatured proteins were removed by centrifugation (14,000 rpm for 30 min) at 4°C, and the supernatant solution was used as the crude extract for purification. The crude extract was desalted through a HiPrep 26/10 desalting column (Amersham-Biosciences) and applied onto a SuperQ TOYOPEARL 650M column (Tosoh) equilibrated with 20 mM Tris-HCl buffer, pH 8.0. The protein was eluted with a linear gradient of 0–0.3 M NaCl. The fraction containing the protein was desalted with HiPrep 26/10 with 20 mM Tris-HCl buffer, pH 8.0 and subjected to a RESOURCE Q column (Amersham-Biosciences) equilibrated with the same buffer. The protein was eluted with a linear gradient of 0–0.3 M NaCl. The fraction containing the protein was desalted with HiPrep 26/10 containing 10 mM sodium phosphate buffer, pH 7.0, and applied onto a Bio-Scale CHT-20-I column (BIO-RAD) equilibrated with the same buffer. The protein was eluted with a linear gradient of 10–100 mM phosphate, pH 7.0. The fractions containing the protein were pooled, concentrated by ultrafiltration (Amicon, 5k cut), and loaded onto a HiLoad 16/60 Superdex 200 pg column (Amersham-Biosciences) equilibrated with 20 mM Tris-HCl buffer, pH 8.0, containing 0.2 M NaCl. The purified protein showed a single band on SDS-polyacrylamide gel electrophoresis. The concentration of the protein was estimated from the absorbance at 280 nm, assuming $E^{1cm}_{1\%}$ = 10.57 as calculated from the molar absorption coefficient.

Table 1. **X-ray crystallographic data and refinement statistics for *Tt*PRAI.**

Data collection*	
X-ray source	SPring-8 BL26B1
Wavelength (Å)	1.00000
Temperature (K)	100
Space group	$P4_132$
Cell parameters	$a = b = c = 144.205$ (Å)
	$\alpha = \beta = \gamma = 90$ (degree)
Resolution (Å)	35.0–2.00 (2.07–2.00)
No. of observed reflections	307,402
No. of unique reflections	35,156
R_{merge}	0.080 (0.763)
Completeness	0.998 (0.994)
Redundancy	8.7 (5.0)
$I/\sigma I$	9.92 (3.00)
Mosaicity (deg)	0.34
Wilson B (Å^2)	29.43
No. of molecules in a.s.u.	2
V_m	2.7
Refinement	
No. of protein atoms	3,058
No. of water molecules	301
Average B factor (Å^2)	44.9
r.m.s. bond distance (Å)	0.007
r.m.s. bond angle (degree)	1.3
R** (35.0–2.00 Å)	0.262
R_{free}*** (35.0–2.00 Å)	0.296
Ramachandran plot (%)	
favored	89.2
allowed	10.2
generous	0.6
disallowed	0.0

*Values in parentheses are for the highest resolution shell. **R was calculated from the working set (95% of the data). ***R_{free} was calculated from the test set (5% of the data).

Crystallization—The protein crystal used for data collection had a size of 0.3 × 0.2 × 0.1 mm^3 and was obtained using the oil microbatch method by TERA (*14*). A 0.5 μl aliquot of protein solution (29.63 mg ml^{-1} in 20 mM Tris-HCl, pH 8.0, 0.2 M NaCl) was mixed with an equal volume of reservoir solution (27.5% isopropanol buffered with 0.1 M sodium acetate, pH 5.1) and covered with 15 μl of paraffin oil. Block-shaped single crystals appeared after two days of incubation at 22°C.

Data Collection and Structure Determination—X-ray diffraction data were collected at beamline BL26B1, SPring-8, Harima, Japan. The crystal with Paratone-N and 10% w/v glycerol as the cryoprotectant was flash-cooled in a 100 K dry nitrogen stream. The data were processed using the programs *DENZO* and *SCALEPACK* (*15*). The crystals belonged to the space group $P4_132$, with a dimer in the asymmetric unit, a solvent content of

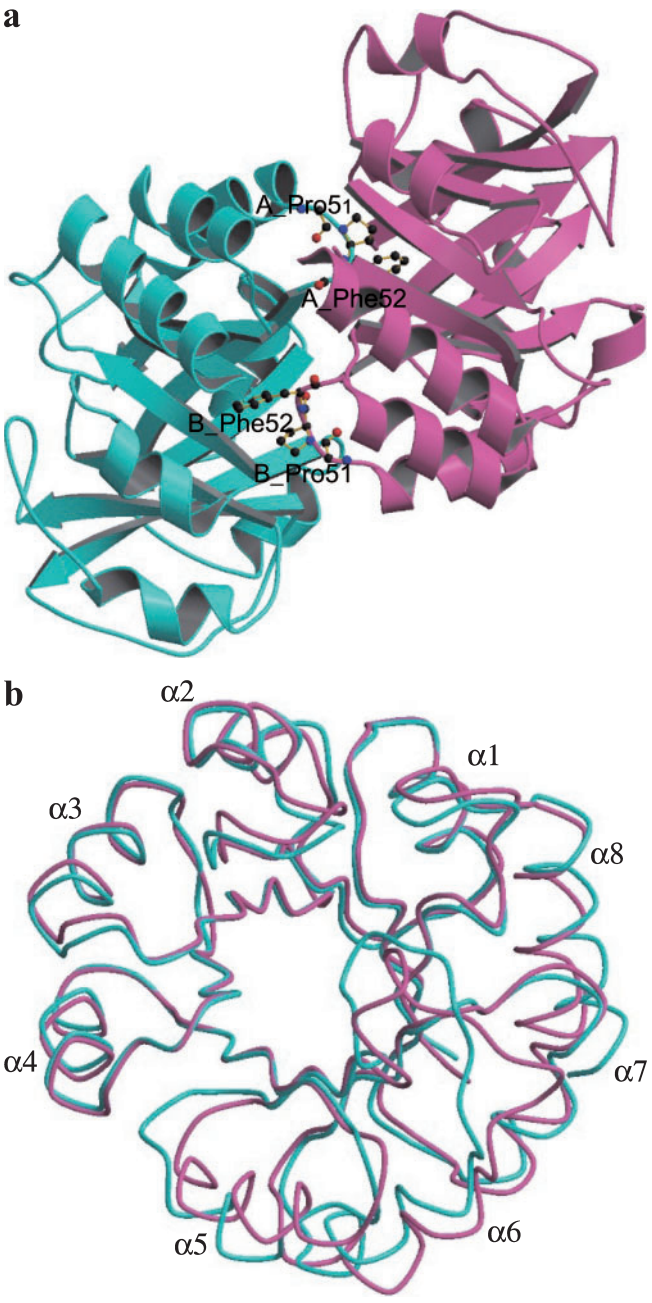

Fig. 1. **(a) Schematic view of the crystal structure of dimeric *Tt*PRAI.** The *A* and *B* subunits are depicted in cyan and red, respectively. Two loops containing Pro51 and Phe52 protrude reciprocally into the cavities of the two fold related subunit. **(b) Structure comparison of *Tt*PRAI and *Tm*PRAI.** Schematic view of *Tt*PRAI and superimposed *Tm*PRAI using 197 equivalent Cα atoms. Cyan and red represent the structures of *Tt*PRAI and *Tm*PRAI, respectively. α1 to α8 represent helix 1 to helix 8, respectively.

54.7%, and a specific volume V_M of 2.7 A^3 Da^{-1} (*16*). Phases were estimated by the molecular replacement method using the program *AMoRe* (*17*). The refined structure of *Tm*PRAI (PDB code 1NSJ) was used as the search model. The positional and temperature-factor refinement with strict noncrystallographic symmetry constraints was performed using the program *CNS* (*18*). The structure was revised manually using the program

Table 2. **Comparison of the amino acid compositions of three phosphoribosyl anthrnilate isomerase.**

	*Tt*PRAI		*Tm*PRAI		*Ec*PRAI	
	Residue	(%)	Residue	(%)	Residue	(%)
Hydrophobic	132	65.0	109	53.2	110	55.6
Gly	19	9.4	14	6.8	21	10.6
Ala	34	16.7	13	6.3	28	14.1
Val	14	6.9	23	11.2	19	9.6
Leu	27	13.3	17	8.3	22	11.1
Ile	7	3.4	14	6.8	6	3.0
Met	3	1.5	3	1.5	1	0.5
Phe	7	3.4	12	5.9	6	3.0
Trp	3	1.5	1	0.5	2	1.0
Pro	18	8.9	12	5.9	5	2.5
Neutral	13	6.4	30	14.6	41	20.7
Ser	5	2.5	14	6.8	9	4.5
Thr	2	1.0	4	2.0	6	3.0
Asn	1	0.5	8	3.9	9	4.5
Gln	4	2.0	2	1.0	13	6.6
Cys	1	0.5	2	1.0	4	2.0
Hydrophilic	58	28.6	66	32.2	47	23.7
Asp	5	2.5	12	5.9	12	6.1
Glu	22	10.8	17	8.3	10	5.1
Lys	6	3.0	13	6.3	7	3.5
His	1	0.5	2	1.0	4	2.0
Arg	20	9.9	15	7.3	8	4.0
Tyr	4	2.0	7	3.4	6	3.0
Total Res.	203		205		198	

QUANTA (Accelrys). After rebuilding, the structure was refined without the non-crystallographic symmetry constraints. The refined model consists of 3,058 protein atoms and 301 water molecules in an asymmetric unit. The electron density of the C-terminal tail of each monomer, comprising residues 201–203, was not visible. The X-ray crystallographic data and refinement statistics are summarized in Table 1. The final coordinates have been deposited in the Protein Data Bank (PDB code 1V5X).

Differential Scanning Calorimetry—DSC was carried out with a differential scanning calorimeter, MicroCal VP-DSC (Northanmpton, USA). Prior to the measurements, the protein solution was dialyzed against the buffer used. The dialyzed sample was filtered through a 0.22-μm pore size membrane and then degassed in a vacuum. The buffers used in the presence of 0.1 mM EDTA were 50 mM glycine in the acidic region and 50 mM potassium phosphate in the neutral region. The protein concentrations under measurement were 0.8–1.5 mg ml^{-1}. The DSC curves were analyzed using the Origin software from MicroCal.

Analytical Ultracentrifugation—Sedimentation equilibrium experiments were carried out using a Beckmann Optima mode XL-A at 20°C with an An-60 Ti rotor at a speed of 12 K or 18 K rpm. Prior to the measurements, the protein solutions were dialyzed overnight against the respective buffer at 4°C. Experiments at three different protein concentrations between 1.8 and 0.5 mg ml^{-1} were performed in Beckman 4-sector cells. The buffers used in the presence of 0.1 mM EDTA were 50 mM glycine in the acidic region and 50 mM potassium phosphate in the neutral region. The partial specific volume of 0.757 cm^3 g^{-1}

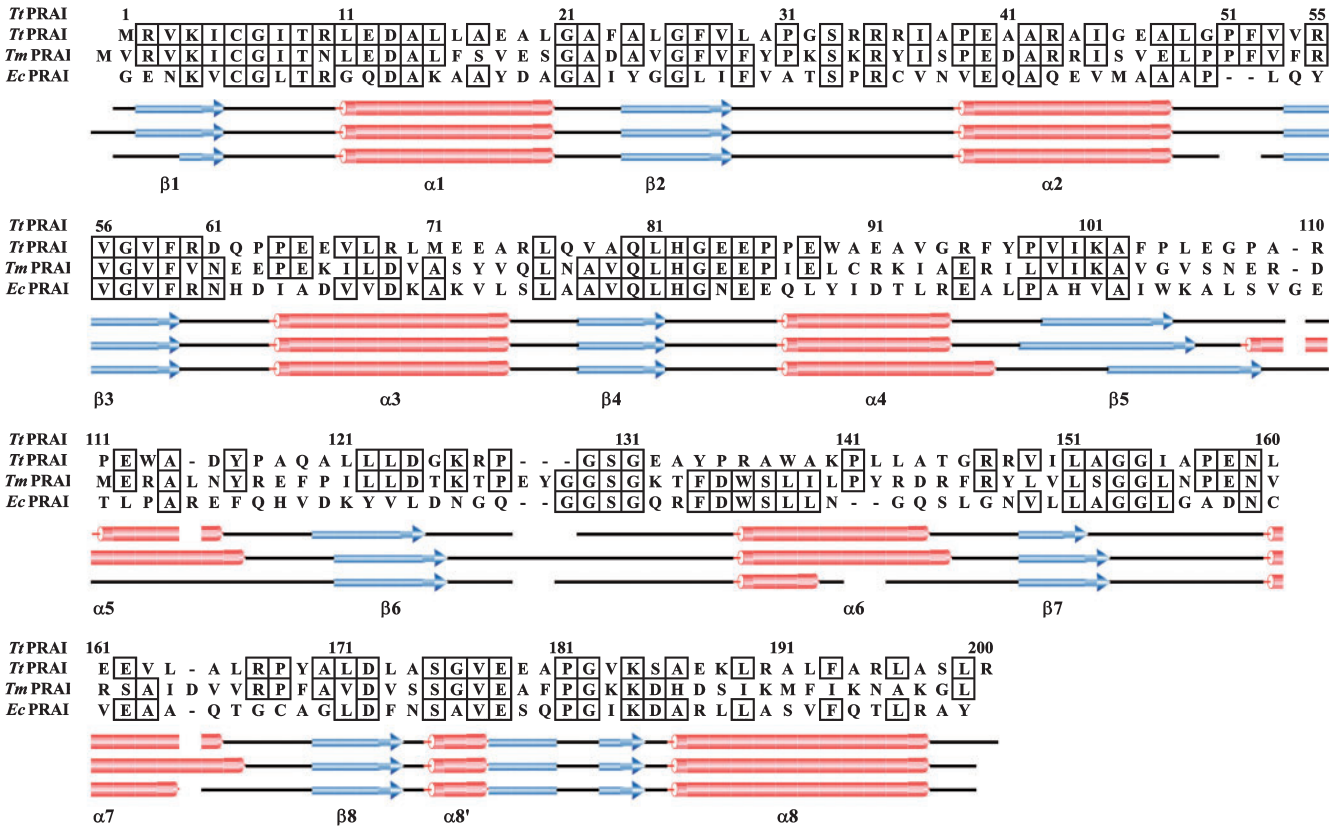

Fig. 2. **Structure based sequence alignments of the three PRAIs from *T. thermophilus, T. maritima,* and *E. coli.*** The first line shows the residue number of *Tt*PRAI. The second, third, and fourth lines are the amino acid sequences of *Tt*PRAI, *Tm*PRAI, and *Ec*PRAI, respectively. The fifth, sixth, and seventh lines indicate secondary structural elements of *Tt*PRAI, *Tm*PRAI, and *Ec*PRAI, respectively, as judged from the secondary structure definition as established by DSSP [9]. Red blocks, blue arrows, black bars, and spaces indicate helices including 3_{10}-helix, β-strand, other secondary structures, and deleted residues, respectively. The eighth line represents the alias of secondary segments named by Henning *et al.* (*5*). Boxes indicate residues conserved in more than two proteins.

used for *Tt*PRAI was based on the amino acid composition of the protein (*19*). Analysis of the sedimentation equilibrium was performed using the program "XLAVEL" (Beckman, version 2.0).

CD Measurements—CD spectra were measured at 25°C with a Jasco-J720 spectropolarimeter. Far- and near-UV CD spectra were scanned 16 and 32 times, respectively, at a scan rate of 20 nm min^{-1}, using a time constant of 0.25 s. The light path length of the cell used was 1.0 mm in the far-UV region and 10 mm in the near-UV region. The buffers used in the presence of 0.1 mM EDTA were 50 mM glycine in the acidic region and 50 mM potassium phosphate in the neutral region. The protein concentrations were 0.1–1.35 mg ml^{-1}. For the calculation of mean residue ellipticity, [θ], the mean residue weight was assumed to be 108.1.

RESULTS AND DISCUSSION

Quality of the Model and Overall Structure of TtPRAI—The refinement of *Tt*PRAI structure converged to an *R* factor of 26.2% and a free *R* value of 29.6% for reflections in the resolution range of 35.0–2.0Å. The current model is a dimer with 200 residues in each subunit. The refined structure model of *Tt*PRAI converged well with root mean square deviations (rmsd) from the ideal bond length and angle of 0.007 Å and 1.30°, respectively. 89.2% of the non-glycine and non-proline residues were in the most favorable region of the Ramachandran plot, 10.2% in the additionally allowed region, 0.6% in the generously allowed region, and no residues in the disallowed region (Table 1).

The monomer structure of *Tt*PRAI adopts an 8-fold α/β barrel fold, as first observed for a triose-phosphate isomerase (*20*). As shown in Fig. 1a, two subunits of *Tt*PRAI associate *via* the N-terminal faces of their central barrels related by a non-crystallographic two-fold axis. Two symmetry-related long loops (including Pro51 and Phe52) protrude reciprocally into cavities of the other subunit, which is similar to what is observed for *Tm*PRAI (*5*). All the residues of *Tt*PRAI dimer are visible in the electron density except for the three C-terminal residues (201–203). The structures of the two subunits of *Tt*PRAI are substantially the same, as indicated by the low rmsd after structural superposition of 0.36 Å between their corresponding Cα atoms. However, the average *B*-factors of the main chain atoms of the subunits differ from each other: 54.93 and 30.58 $Å^2$ for the *A* and *B* chains, respectively. The different *B*-factors of the two subunits might be a consequence of their different packing in the crystal. The high *R*- and free *R*-factors, despite

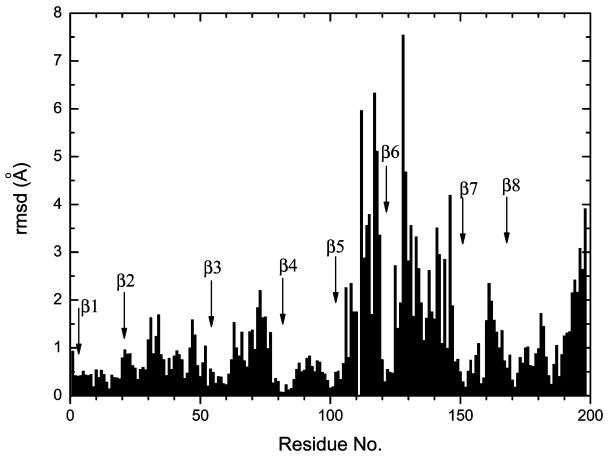

Fig. 3. **Rms deviations of Cα atoms between *Tt*PRAI and *Tm*PRAI after a least squares fitting of 197 corresponding Cα atoms.** Residue numbers of *Tt*PRAI are shown. Arrows show the positions of β-sheets.

the good quality diffraction data, might be caused by the high *B*-factors of the *A* chain.

Amino Acid Compositions—*Tt*PRAI and *Tm*PRAI consist of 203 and 205 residues, respectively. The number of amino acid residues in PRAI from *E. coli* (*Ec*PRAI), which is a domain corresponding to the phosphoribosyl anthranilate isomerase in a bifunctional enzyme, is 198. Table 2 shows the amino acid compositions of the three proteins. The proportion of hydrophobic residues in *Tt*PRAI (132; 65.0%) is greater than that in *Tm*PRAI (109; 53.2%); especially, the levels of Ala and Leu are remarkably different. On the other hand, the number of neutral residues in *Tt*PRAI is less than half those in the other two proteins. The number of ionizable residues in the thermophilic proteins (*Tt*PRAI and *Tm*PRAI) is greater than in the mesophilic protein (*Ec*PRAI), suggesting a contribution of ion-bonds to the thermo-stabilization of thermophilic proteins.

Structural Comparison—Figure 2 shows the secondary structure-based sequence alignment of the three proteins using the secondary structural elements assigned with DSSP (*21*). The residue identity between *Tt*PRAI and *Tm*PRAI is 40.4% (82/203), and that between *Tt*PRAI and *Ec*PRAI is 25.1% (51/203). The alignment indicates that the mesophilic protein, *Ec*PRAI, has a deletion of two residues at positions 51 and 141 of *Tt*PRAI, and the insertion of one residue at position 109 of *Tt*PRAI. These changes are conserved in both thermophilic proteins.

Figure 1b shows the backbone structures of *Tt*PRAI and superimposed *Tm*PRAI using 197 equivalent Cα atoms. All of the β strands and some of the α helices seem to be structurally identical. The rmsd between the 197 Cα atoms of *Tt*PRAI and *Tm*PRAI is 1.17 Å. The region showing the highest deviations, as shown in Fig. 3, belongs to the flexible loop (residues Gly125–Pro135) that connects strand β6 and helix α6 (loop β6α6). The following might cause this large deviation. (i) Three residues between residues Pro130 and Gly134 of *Tm*PRAI are absent from the loop β6α6 of *Tt*PRAI. (ii) All residues in the loop of *Tt*PRAI are visible in the electron density, while those of the *Tm*PRAI have been reported to be invisible (*5*). The second large deviation that includes residues Glu106–Gln119 consists of loop β5α5 and helix α5. The deviations between the Cα atoms for each class of secondary structure of *Tt*PRAI and *Tm*PRAI were calculated to be 0.46 (42 atoms), 1.35 (73), and 1.37 (82) Å for β strand, α helix, and others, respectively. The structures of *Tt*PRAI and *Ec*PRAI were also superimposed with an rmsd of 1.40 Å between 181 equivalent Cα atoms in both proteins, and the deviations for each class of secondary structure were 0.62 (42 atoms), 1.60 (66), and 1.32 (78), respectively. These results indicate that the deviations in β-strands among the three proteins are the lowest. Arrows in Fig. 3 indicate the positions of the β strands, where deviations are clearly lower than those in other positions. These results suggest that the β sheet structures in the $(\beta\alpha)_8$ barrel structure of PRAI are more conserved than other secondary structural elements. The conservation in the β sheet structure seems to be rational, because the β barrel, comprising the central architecture in the $(\beta\alpha)_8$ barrel fold, and β-strands are directly hydrogen bonded to each other in the center of the molecules, whereas the α-helices are connected to the β-strands by loop regions.

Dimer Interface—It has been suggested that the two loops α2β3 of the *Tm*PRAI dimer provide an unusual mode of interlocking interaction that is responsible for the high stability of the protein (*5*). The three hydrophobic residues (Pro51-Phe52-Val53) in loops α2β3 of *Tt*PRAI dimer protrude reciprocally into the interior of the β-barrel of the neighboring subunit. The corresponding residues of *Tm*PRAI are Pro52, Phe53, and Val54, which are completely inaccessible to solvent. Pro52 and Phe53 of one subunit of *Tt*PRAI fit into the bottom (0) layer of the barrel (*4*) and the first regular layer, respectively, of the other subunit. The protrusion of these two residues might be important for the stability of the dimer.

The N-terminal (Met1) and C-terminal (Leu205) residues of both subunits of *Tm*PRAI form a hydrophobic cluster at the dimer interface. In the case of *Tt*PRAI, however, the residue corresponding to the N-terminal Met residue of *Tm*PRAI is missing, and the three C-terminal residues (201–203) are flexible and not visible in the electron density. Instead, Arg200 of *Tt*PRAI can be superimposed on the C-terminal residue (Leu205) of *Tm*PRAI. The contribution of terminal residues to the stabilization of the dimer seems to be weaker in *Tt*PRAI than in *Tm*PRAI.

Table 3. **Numbers of ion pairs and hydrogen bonds in *Tt*PRAI, *Tm*PRAI and *Ec*PRAI.**

		*t*PRA I (inter-subunit)		*m*PRAI (inter-subunit)		*Ec*PRAI
Number of ion pairs	<3 Å	6	(2)	6	(2)	5
	<4 Å	19	(4)	20	(4)	14
	<5 Å	31	(4)	26	(4)	19
Number of hydrogen bonds		191	(15)	195	(12)	192

Table 4. **Contribution of each stabilizing factor to the stabilities of the three proteins on the basis of structural information.** $\Delta\Delta G_{HP}$ and $\Delta\Delta G_{CAV}$ represent the difference in ΔG values between two proteins due to changes in hydrophobic interactions and cavity volume, respectively. A positive ΔG indicates stabilization.

Proteins	*Tt*PRAI*	*Tm*PRAI**	*Ec*PRAI***
ASA value of the N state (Å^2)			
C/S atoms	5,030	5,142	4,445
N/O atoms	4,197	4,848	4,705
ASA value of the D state (Å^2)			
C/S atoms	18,201	18,239	16,636
N/O atoms	9,294	10,095	10,009
Difference of *ASA* (D–N) (Å^2)			
C/S atoms	13,171	13,097	12,191
N/O atoms	5,097	5,247	5,304
ΔG_{HP} (kJ/mol)	1,896	1,881	1,740
$\Delta\Delta G_{HP}$ (kJ/mol)****	0	–15	–56
Surface area buried at dimer interface (Å^2)			
C/S atoms	1,440	1,765	
N/O atoms	1,074	1,306	
ΔG_{HP} (kJ/mol)	194	238	
$\Delta\Delta G_{HP}$ (kJ/mol)****	0	44	
Cavity volume			
monomer (dimer) (Å^3)	80 (312)	15 (76)	
ΔG_{CAV} (kJ/mol)	–4.2 (–16.2)	–0.8 (–4.0)	
$\Delta\Delta G_{CAV}$ (kJ/mol)****	0	3.4 (12.2)	

*Chain B of protein 1V5X was used for calculation. **1NSJ. ***Structure from Gly255 to Tyr452 in 1PII. ****Subtracted from the value of Tt PRAI.

The accessible surface area (*ASA*) of the dimer interface was calculated (Table 4). The total surface area buried at the dimer interface of *Tt*PRAI was only 81.9% that of *Tm*PRAI, suggesting a difference in the hydrophobic interactions between the two thermophilc PRAIs described later.

Active Site—The active site of *Ec*PRAI is speculated to be covered by four long loops, β2α2, β5α6, β6α6, and β8α8 (including helix α8′) on the C-terminal side of the central β-barrel (*2*). Electron density indicative of a phosphate ion has been observed at the potential binding sites of the phosphate-ester moiety of the substrate phosphoribosyl anthranilate in *Ec*PRAI. Although the electron density of a phosphate ion was not detected at the equivalent position in *Tt*PRAI, the superimposition of the two structures near the phosphate ion binding site for *Tt*PRAI and *Tm*PRAI reveals no significant differences, suggesting a conservation of structure near the active sites. Electron density for a phosphate ion might be observed at the corresponding site in *Tt*PRAI if the crystallization cocktail contained phosphate ions.

Ion Pairs (Salt Bridges) and Hydrogen Bonds—It is believed that ion pairs (salt bridges) play an important role in the stability of proteins from hyperthermophiles, because they occur so frequently. The number of ion pairs within 4 Å in *Tt*PRAI is comparable to that in *Tm*PRAI, which is greater than that in the mesophilic protein, *Ec*PRAI (Table 3). The number of inter-subunit ion pairs of *Tt*PRAI and *Tm*PRAI is the same, but their positions differ. Arg148 in *Tt*PRAI pairs with Glu18 (α1) of the another subunit, and the corresponding Arg152 in *Tm*PRAI bonds with Glu49 in a different secondary structural segment (α2). This change results in the area of subunit interface in *Tt*PRAI being less than that in *Tm*PRAI, which also weakens the hydrophobic interaction of the dimer interface of *Tt*PRAI as described below. Table 3 lists the number of hydrogen bonds in the three proteins. The total numbers of hydrogen bonds shorter than 3.3 Å in the three proteins are almost the same, except for those of the dimer interface in thermophilic proteins.

Hydrophobic Interaction—The hydrophobic effects on the conformational stability of proteins have been extensively analyzed by studies involving site-directed mutagenesis, and it has been revealed that hydrophobic residues in the interior of a protein contribute to conformational stability (*22–24*). Takano *et al.* (*25*) have found a general rule for the relationship between hydrophobic effect and conformational stability, using a series of hydrophobic mutants of human lysozyme. The change in unfolding Gibbs energy (ΔG) due to the hydrophobic effect between the wild-type and mutant proteins ($\Delta\Delta G_{HP}$) can be expressed as follows:

$$\Delta\Delta G_{HP} = \alpha\Delta\Delta ASA_{non\text{-}polar} + \beta\Delta\Delta ASA_{polar} \quad (1)$$

where $\Delta\Delta ASA_{non\text{-}polar}$ and $\Delta\Delta ASA_{polar}$ represent the difference in ΔASA of the non-polar and polar atoms of all residues, respectively, between the wild-type and mutant proteins upon denaturation. Parameters α and β have been determined to be 0.154 and –0.026 kJ mol^{-1} Å^{-2}, respectively, using the stability/structure database of mutant human lysozymes (*26*). For calculation of the *ASA* value, carbon and sulfur atoms in the residues are assigned as $ASA_{non\text{-}polar}$, and nitrogen and oxygen atoms as ASA_{polar}.

The contribution of hydrophobic interactions in the three proteins to the stabilization of the proteins and of

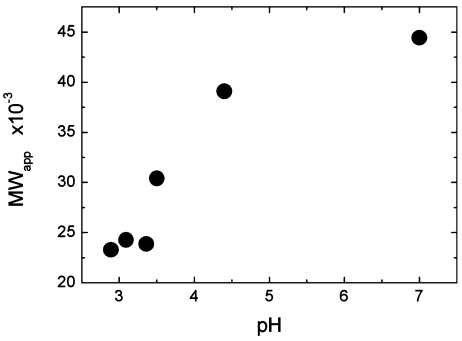

Fig. 4. **pH dependence of the apparent molecular weight (MW_{app}) of *Tt*PRAI.** Each data point shows the average value of three different concentrations (0.3 mg ml^{-1} to 1.0 mg ml^{-1}) at 20°C. Potassium phosphate, acetate, and glycine buffers (50 mM) were used at pH 7.0, pH 4.4, and below pH 3.5, respectively.

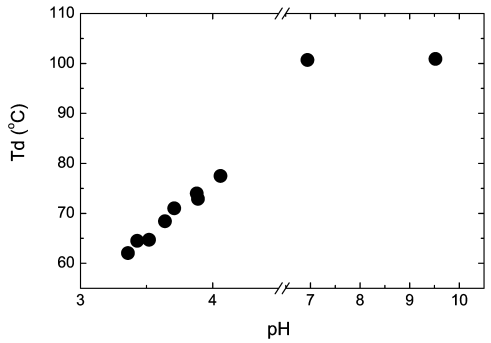

Fig. 5. **pH dependence of the denaturation temperature of *Tt*PRAI.** The denaturation temperature, Td, represents the temperature corresponding to the peak of the DSC curve observed at a scan rate of 1°C min^{-1}. pH indicates values after DSC measurements. Potassium phosphate and acetate buffers (50 mM) were used at pH 7.0 and pH 4.4, respectively, and 50 mM glycine buffer was used at pH 9.5 and below pH 3.5.

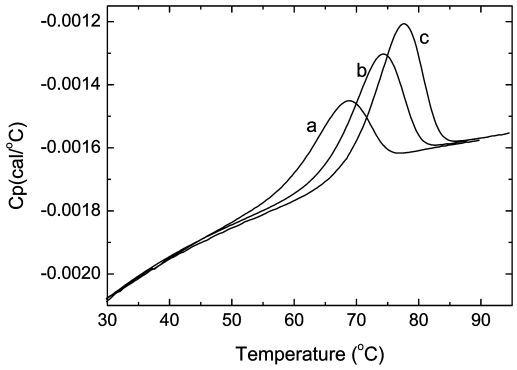

Fig. 6. **Typical DSC curves of *Tt*PRAI in the acidic region.** (a), (b), and (c) represent excess heat capacity curves at pH 3.64, 3.88, and 4.06, respectively. The DSC measurements were performed at scan rate of 1°C min^{-1}.

the dimer interface of the two thermophilic proteins were estimated using Eq. 1. The *ASA* values of the native state were calculated by the procedure of Connolly (*27*) using the X-ray structures of the three proteins. The *ASA* values for the denatured forms were estimated using extended structures of each protein generated from the native structures using the program Insight II. The contribution of hydrophobic interactions to the stability of the three proteins is shown in Table 4. In the monomer structure, the hydrophobic interaction ($\Delta\Delta G_{HP}$) of *Tt*PRAI is higher by 15 and 56 kJ mol^{-1} than those of *Tm*PRAI and *Ec*PRAI, respectively. But the $\Delta\Delta G_{HP}$ value originating from the hydrophobic interaction at the dimer interface of *Tm*PRAI is remarkably higher (44 kJ mol^{-1}) than that of *Tt*PRAI. This means that *Tm*PRAI is more stabilized by hydrophobic interactions than *Tt*PRAI in total, although the proportion of hydrophobic residues in *Tm*PRAI was lower than that in *Tt*PRAI (Table 2).

Cavity Volume—Changes in the cavity volume in the interior of a protein affect its conformational stability (*28*). Therefore, the cavity volumes of the three proteins were estimated using a probe sphere of 1.4 Å radius (corresponding a water molecule) (*27*). The cavity volumes of *Tt*PRAI in the monomer and dimer states are greater than those of *Tm*PRAI (Table 4). The energy contribution to protein stability (ΔG_{CAV}) due to changes in the cavity size can be expressed in terms of the cavity volume (52 J mol^{-1} Å^{-3}) (*26*). Using this parameter, the increment of stabilization ($\Delta\Delta G_{CAV}$) of *Tm*PRAI in the monomer and dimer states due to the change in cavity volume was calculated to be 3.4 and 12.2 kJ mol^{-1}, respectively (Table 4), compared with those of *Tt*PRAI. The difference in the contribution of the change in cavity volume to stability at the interface between *Tt*PRAI and *Tm*PRAI was estimated to be 5.4 (= 12.2 – 3.4 × 2) kJ mol^{-1}, after subtracting the contribution of the monomer structure from that of a dimer structure.

Molecular Assembly Forms of TtPRAI at Different pHs—It has been reported that *Tm*PRAI is a homodimer in solution even at pH 3.2 (*9*), although *Ec*PRAI which is part of a bifunctional chain, is monomeric. Therefore, ultracentrifugation experiments of *Tt*PRAI were performed at neutral and acidic pHs at 20°C to examine the molecular assembly forms at different pHs. As shown in Fig. 4, *Tt*PRAI is a dimer at pH 7.0 (MW of a monomer = 21.95k) but dissociates to monomers below pH 3.4. This suggests that the dimeric association of *Tt*PRAI is weaker than that of *Tm*PRAI at pH 3.2.

Differential Scanning Calorimetry of TtPRAI—To verify whether the association-dissociation between the subunits in *Tt*PRAI is related to the change in stability, the heat stabilities of *Tt*PRAI were measured by DSC at the scan rate of 1°C min^{-1} in the pH region where the dissociation occurs (Fig. 4). The apparent denaturation temperatures above neutral pH were around 100°C (Fig. 5). DSC measurements could not be carried out between pH 6.5 and pH 4.5, near the isoelectric point of the protein, because the protein became turbid upon heating. Below pH 4.5, the denaturation temperatures decreased markedly with decreasing pH (Fig. 5). Above pH 3.6 the excess heat capacity changes in the DSC curves could be clearly observed as shown in Fig. 6. However, no excess heat capacity was found below pH 3.3, suggesting that the protein was acid-denatured.

In the DSC measurements of the cooling and reheating processes after the first heating, no excess heat capacity curve was observed in the acidic region, suggesting that the heat denaturation of *Tt*PRAI was not reversible

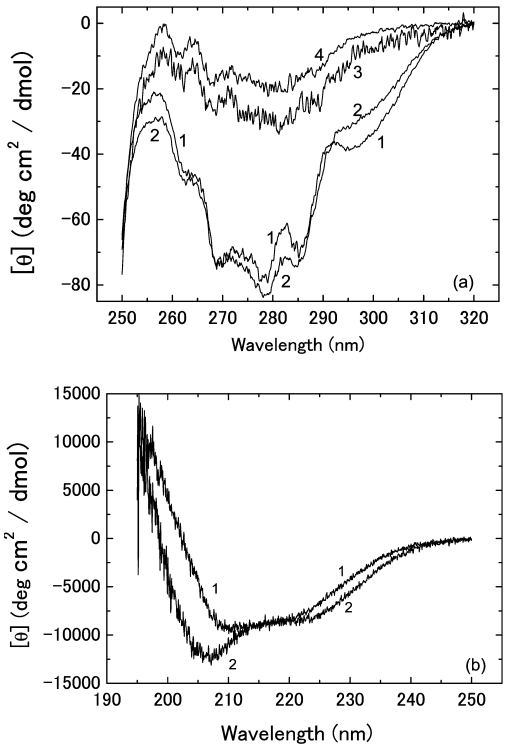

Fig. 7. **CD spectra of *Tt*PRAI in the near- (a) and far- (b) UV region at 25°C.** (a) Curves 1, 2, 3, and 4 represent spectra at pH 7.0, 3.8, 3.4, and 3.1, respectively. (b) Curves 1, and 2 represent spectra at pH 7.0 and pH 3.1, respectively.

under the conditions of the experiment. Furthermore, when the scan rate of DSC was decreased at pH 3.7, the denaturation temperature also decreased: denaturation temperatures were 68.4, 66.5, and 63.0°C for scan rates of 1.0, 0.5, and 0.25°C min^{-1}, respectively. These results indicate that the denaturation of *Tt*PRAI is quite slow and does not reach equilibrium. It has been reported that the denaturation rates of hyperthermophilic proteins are unusually slow (*29–33*). For example, the heat denaturation of pyrrolidone carboxyl peptidase from the hyperthermophile *Pyrococcus furiosus* does not reach equilibrium even at a very slow scan rate of 1°C h^{-1}, and is under kinetic control (*34*). *Tt*PRAI from the extreme thermophile also has this common feature of hyperthermophilic proteins.

CD Spectra of TtPRAI in the Acidic pH—In order to examine the state of the structure of *Tt*PRAI around pH 3, CD spectra in the near and far-UV region were measured. Changes in the tertiary structure of a protein can be judged from the near-UV CD spectrum (from 250 to 320 nm), which originates from aromatic side-chains. Curve 3 in Fig. 7a suggests that the tertiary structure of *Tt*PRAI is largely destroyed at pH 3.4 as compared with curve 1 at pH 7.0. However, the structure at pH 3.8 seems to be still intact because the CD spectrum is quite similar to that at pH 7.0, as shown in Fig. 7a. At pH 3.1, four negative peaks characteristic of the native state disappear (curve 4 in Fig. 7a), indicating that the native structure has become almost completely denatured. On the other hand, as judged from the spectrum in the far-UV region (Fig. 7b), a fairly high content of secondary structure seems to remain at pH 3.1. Although the CD values at 220 nm at pH 3.1 are similar to those at pH 7.0, the negative values around 205 nm at pH 3.1 are significantly larger than that at pH 7.0 in the native state. The results of the CD and DSC measurements indicate that the structure of *Tt*PRAI undergoes thermodynamically denaturation at pH 3.1, although the secondary structure still remains. This is in agreement with the characteristics of a molten globule structure already reported (*35*).

Stabilization Due to Dimer Formation in TtPRAI—The apparent denaturation temperature of *Tt*PRAI from *T. thermophilus*, which is an extremely thermophilic eubacterium with a maximum growth temperature of 85°C, is around 100°C above pH 7 (Fig. 5). The stability of this protein might be comparable to or less than that of *Tm*PRAI, because *Tm*PRAI originates from a hyperthermophile, *T. maritima*, which has a higher maximum growth temperature of 90°C than that of *T. thermophilus*. Now, we can compare the stabilization factors of both proteins on the basis of their crystal structures. In the case of monomer structures, (i) the hydrophobic interaction ($\Delta\Delta G_{HP}$) of *Tt*PRAI is only slightly higher than that of *Tm*PRAI (Table 4), (ii) the number of hydrogen bonds does not differ among the three proteins (Table 3), (iii) the number of ion bonds is slightly greater in the thermophilic proteins than in the mesophilic protein (Table 3), and (iv) the cavity volume of *Tt*PRAI is greater than that of *Tm*PRAI (Table 4). As compared with the mesophilic protein (*Ec*PRAI), the thermophilic proteins (*Tt*PRAI and *Tm*PRAI) seem to be stabilized by hydrophobic interactions and ion bonds. No large difference in stabilization between the thermophilic proteins was evident at the level of the monomer structures.

At the subunit interface, however, hydrophobic interactions and a decrease in the cavity volume contribute less to the stability of *Tt*PRAI than that of *Tm*PRAI (Table 4). The number of hydrogen bonds in *Tt*PRAI is slightly higher than in *Tm*PRAI, but the number of ionic bonds is the same. These results suggest that the dimer form of *Tt*PRAI is less stable than that of *Tm*PRAI.

From the present experiments, it is evident that the acid denaturation of *Tt*PRAI correlates to the dissociation of a dimer form, and an intact monomer structure can not be maintained below pH 3.5. On the other hand, in the case of *Tm*PRAI, based on sedimentation equilibrium and CD experiments, it has been reported that the protein with a molecular weight of a dimer form is not denatured at pH 3.2 (*9*). This implies that the *Tm*PRAI is more stable than the *Tt*PRAI at pH 3.2. This agrees with the above conclusion based on the difference in structures at the dimer interfaces of these proteins.

Henning *et al.* (*5*) have proposed the possibility that the sequential hydrophobic residues (Pro51-Pro52-Phe53-Val54) in loop α2β3 of *Tm*PRAI, which protrude reciprocally into the interior of the β-barrel of the neighbouring subunit, are responsible for the stability of the dimer. They found that only PRAI from the halophilic archaeon *Halofearax volcanii* among all PRAI sequences available at that time has the same hydrophobic amino acid sequence as PPFV of *Tm*PRAI. Therefore, only "extremophilic" PRAIs seemed to be stabilized by dimerization *via* these residues. However, recently, when all PRAI sequences available in the Swissprot databank were

aligned, it was found that the PRAIs from many mesophiles have the same sequence (LPPFV) as that (from Leu50 to Val53) of *Tm*PRAI. Therefore, attempts were made to predict the tertiary structures of several PRAIs from mesophiles containing the LPPFV sequence by homology modeling using MOE software (Chemical Computing Group Inc.). All predicted structures could be superimposed very well with those of *Tt*PRAI and *Tm*PRAI at the dimer interface (not shown). These results suggest that these mesophilic proteins form homodimers and that the hydrophobic sequence LPPFV is not a unique characteristic of thermophilic proteins such as the *Tm*PRAI.

The sequence Leu49-Gly50-Pro51-Phe52-Val53 of *Tt*PRAI corresponds to the LPPFV of *Tm*PRAI. The Gly50 of *Tt*PRAI is not observed in *Tm*PRAI. Pro51 and Phe52 in the protrusion of *Tt*PRAI seem to be the most important residues contributing to the dimeric structure, because they are trapped in the other subunit as shown in Fig. 1. Although this protrusion might be important for preserving the dimeric form, many other factors should also be responsible for the higher stability of the dimer in thermophiles as revealed by the differences in the stabilizing factors between *Tt*PRAI and *Tm*PRAI demonstrated in the present study.

CONCLUSIONS

The crystal structure of *Tt*PRAI was solved at 2.0 Å resolution. The overall structure of *Tt*PRAI is quite similar to that of *Tm*PRAI with a dimeric structure. The *Tt*PRAI also has a hydrophobic protrusion at the subunit interface, which is similar to that of *Tm*PRAI. Therefore, in order to elucidate the role of the protrusion, the stability of *Tt*PRAI has also been investigated by DSC, CD, and analytical centrifugation in the acidic range as it relates to the association-dissociation of the subunits. The denaturation temperature of *Tt*PRAI in solution declined sharply with decreasing pH below pH 4.5. The tertiary structure was largely destroyed at pH 3.4. This denaturation of the protein at acidic pH was correlated with the dissociation of its dimeric form.

On the basis of the crystal structures of proteins from mesophilic, extreme thermophilic, and hyperthermophilic organisms, we found that (i) the hydrophobic interactions of *Tt*PRAI in the monomer structure are greater than those of *Ec*PRAI and *Tm*PRAI, but those at the dimer interface of *Tm*PRAI are remarkably greater; (ii) the contributions of hydrogen bonds to stability among the three proteins are similar, but ion pairs in both thermophilic proteins contributed more to the stability than those in the mesophilic protein; (iii) destabilization due to the presence of cavities in *Tt*PRAI is larger than that of *Tm*PRAI in both the monomer and dimer structures; (iv) the higher stability of *Tm*PRAI due to dimer formation is caused by increase in an area of hydrophobic interaction and a decrease in cavity volume at subunit interface as compared with *Tt*PRAI.

The expression plasmid of the protein was supplied by the RIKEN Structurome Group headed by Prof. S. Kuramitsu. We also thank Prof. M. R. N. Murthy for critical reading of the manuscript and Ms. M Sakai for measurements of analytical centrifugation. This work was supported by the RIKEN Structural Genomics/Proteomics Initiative (RSGI), the National Project on Protein Structural and Functional Analyses, Ministry of Education, Culture, Sports, Science, and Technology of Japan.

REFERENCES

1. Jaenicke, R. and Bohm, G. (1998) The stability of proteins in extreme environments. *Curr. Opin. Struct. Biol.* **8**, 738–748
2. Rees, D.C. (2001) Crystallographic analyses of hyperthermophilic proteins. *Methods Enzymol.* **334**, 423–437
3. Petsko, G.A. (2001) Structural basis of thermostability in hyperthermophilic proteins, or there's more than one way to skin a cat. *Methods Enzymol.* **334**, 469–478
4. Wilmanns, M., Priestle, J.P., Niermann, T., and Jansonius, J.N. (1992) Three-dimensional structure of the bifunctional enzyme phosphoribosyl anthranilate isomerase: indole glycerolphosphate synthase from *Escherichia coli* refined at 2.0 Å resolution. *J. Mol. Biol.* **223**, 477–507
5. Hennig, M., Sterner, R., Kirschner, K., and Jansonius, J.N. (1997) Crystal structure at 2.0 Å resolution of phosphoribosyl anthranilate isomerase from the hyperthermophile *Thermotoga maritima*: possible determinants of protein stability. *Biochemistry* **36**, 6009–6016
6. Huber, R., Langworthy, T.A., Konig, H., Thomm, M., Woese, C.R., Sleytr, U.B., and Stetter, K.O. (1986) *Thermotoga maritima* sp. nov. represents a new genus of unique extremely thermophilic eubacteria growing up to 90°C. *Arch Microbiol.* **144**, 324–333
7. Sterner, R., Dahm, A., Darimont, B., Ivens, A., Liebl, W., and Kirschner, K. (1995) $(\beta\alpha)_8$-barrel proteins of tryptophan biosynthesis in the hyperthermophile *Thermotoga maritima*. *EMBO J.* **14**, 4395–402
8. Jaenicke, R., Schurig, H., Beaucamp, N., and Ostendorp, R. (1996) Structure and stability of hyperstable proteins: Glycolytic enzymes from hyperthermophilic bacterium *Thermotoga maritima*. *Adv. Protein Chem.* **48**, 181–269
9. Sterner, R., Kleemann, G.R., Szadkowski, H., Lustig, A., Hennig, M., and Kirschner, K. (1996) Phosphoribosyl anthranilate isomerase from *Thermotoga maritima* is an extremely stable and active homodimer. *Protein Sci.* **5**, 2000–2008
10. Villeret, V., Clantin, B., Tricot, C., Legrain, C., Roovers, M., Stalon, V., Glansdorff, N., and Van Beeumen, J. (1998) The crystal structure of *Pyrococcus furiosus* ornithine carbamoyltransferase reveals a key role for oligomerization in enzyme stability at extremely high temperatures. *Proc. Natl Acad. Sci. USA* **95**, 2801–2806
11. Dams, T. and Jaenicke, R. (1999) Stability and folding of dihydrofolate reductase from the hyperthermophilic bacterium *Thermotoga maritima*. *Biochemistry* **38**, 9169–9178
12. Tanaka, H., Chinami, M., Mizushima, T., Ogasahara, K., Ota, M., Tsukihara, T., and Yutani, K. (2001) X-ray crystalline structures of pyrrolidone carboxyl peptidase from a hyperthermophile, *Pyrococcus furiosus*, and its Cys-free mutant. *J. Biochem.* **130**, 107–118
13. Ogasahara, K., Ishida, M., and Yutani, K. (2003) Stimulated interaction between α and β subunits of tryptophan synthase from hyperthermophile enhances its thermal stability. *J. Biol. Chem.* **278**, 8922–8928
14. Sugahara, M. and Miyano, M. (2002) Development of high-throughput automatic protein crystallization and observation system. *PEN* **47**, 1026–1032
15. Otwinowski, Z. and Minor, W. (1997) Processing of X-ray diffraction data collected in oscillation mode. *Methods Enzymol.* **276**, 307–326
16. Matthews, B.W. (1968) Solvent content of protein crystals. *J. Mol. Biol.* **33**, 491–497
17. Navaza, J. (1994) *AMoRe*: an automated package for molecular replacement. *Acta Crystallogr.* **A50**, 157–163

18. Brünger, A.T., Kuriyan, J., and Karplus, M. (1987) Crystallographic *R* factor refinement by molecular dynamics. *Science* **235**, 458–460
19. Durchschlag, H. (1986) in *Thermodynamic Data for Biochemistry and Biotechnology* (Hinz, H.-J., ed.) Chapt 3, p. 45, Springer-Verlag, Berlin, Heidelberg, New York, Tokyo
20. Banner, D.W., Bloomer, A.C., Petsko, G.A., Phillips, D.C., Pogson, C.I., Wilson, I.A., Corran, P.H., Furth, A.J., Milman, J.D., Offord, R.E., Priddle, J.D., and Waley, S.G. (1975) Structure of chicken muscle triose phosphate isomerase determined crystallographically at 2.5 angstrom resolution using amino acid sequence data. *Nature* **255**, 609–614
21. Kabsch, W. and Sander, W. (1983) Dictionary of protein secondary structure: pattern recognition of hydrogen-bonded and geometrical features. *Bioplolymers* **22**, 2577–2637
22. Yutani, K., Ogasahara, K., Sugino, Y., and Matsusiro, A. (1977) Effect of a single amino acid substitution on stability of conformation of a protein. *Nature* **267**, 274–275
23. Yutani, K., Ogasahara, K., Tsujita, T., and Sugino, Y. (1987) Dependence of conformational stability on hydrophobicity of the amino acid residue in a series of variant proteins substituted at a unique position of tryptophan synthase α-subunit. *Proc. Natl. Acad. Sci. USA* **84**, 4441–4444
24. Kellis, J.T., Nyberg, K., Sali, D., and Fersht, A.R. (1988) Contribution of hydrophobic interactions to protein stability. *Nature* **333**, 784–786
25. Takano, K., Yamagata, Y., and Yutani, K. (1998) A general rule for the relationship between hydrophobic effect and conformational stability of a protein: Stability and structure of a series of hydrophobic mutants of human lysozyme. *J. Mol. Biol.* **280**, 749–761
26. Funahashi, J., Takano, K., and Yutani, K. (2001) Are the parameters of various stabilization factors estimated from mutant human lysozymes compatible with other proteins? *Protein Eng.* **14**, 127–134
27. Connolly, M.L. (1993) The molecular surface package. *J. Mol. Graphics* **11**, 139–141
28. Eriksson, A.E., Baase, W.A., Zhang, X.J., Heinz, D.W., Blaber, M., Baldwin, E.P., and Matthews, B.W. (1992) Response of a protein structure to cavity-creating mutations and its relation to the hydrophobic effect. *Science* **255**, 178–183
29. Ogasahara, K., Lapshina, E.A., Sakai, M., Izu, Y., Tsunasawa, S., Kato, I., and Yutani, K. (1998) Electrostatic stabilization in methionine aminopeptidase from hyperthermophile *Pyrococcus furiosus*. *Biochemistry* **37**, 5939–5946
30. Perl, D., Welker, C., Schindler, Schroder, K., Marahiel, M.A., Jaenicke, R., and Schmid, F.X. (1998) Conservation of rapid two-state folding in mesophilic, thermophilic and hyperthermophilic cold shock proteins. *Nature Struct. Biol.* **5**, 229–235
31. Cavagnero, S., Debe, D.A., Zhou, Z.H., Adams, M.W., and Chan, S.I. (1998) Kinetic role of electrostatic interactions in the unfolding of hyperthermophilic and mesophilic rubredoxins. *Biochemistry* **37**, 3369–3376;
32. Ogasahara, K., Nakamura, M., Nakura, S., Tsunasawa, S., Kato, I., Yoshimoto, T., and Yutani, K., (1998) The unusually slow unfolding rate causes the high stability of pyrrolidone carboxyl peptidase from a hyperthermophile, *Pyrococcus furiosus*: Equilibrium and kinetic studies of guanidine hydrochloride-induced unfolding and refolding. *Biochemistry* **37**, 17537–17544
33. Potekhin, S.A., Ogasahara, K., and Yutani, K. (2000) Transition state of heat denaturation of methionine aminopeptidase from a hyperthermophile. *J. Therm. Anal. Calorim.* **62**, 111–122
34. Kaushik, J.K., Ogasahara, K., and Yutani, K (2002) The unusually slow relaxation kinetics of the folding-unfolding of pyrrolidone carboxyl peptidase from a hyperthermophile, *Pyrococcus furiosus*. *J. Mol. Biol.* **316**, 991–1003
35. Yutani, K., Ogasahara, K., and Kuwajima, K. (1992) The absence of the thermal transition in apo-α-lactalbumin in the molten globule state: A study by differential scanning microcalorimetry. *J. Mol. Biol.* **228**, 347–350